Title	Shape control of surface-stabilized disclination loops in nematic liquid crystals
Author(s)	Sunami, Kanta; Imamura, Koki; Ouchi, Tomohiro et al.
Citation	Physical Review E. 2018, 97(2), p. 020701-020701
Version Type	VoR
URL	https://hdl.handle.net/11094/75689
rights	Copyright (2018) by the American Physical Society
Note	

Shape control of surface-stabilized disclination loops in nematic liquid crystals

Kanta Sunami,[1] Koki Imamura,[1] Tomohiro Ouchi,[1] Hiroyuki Yoshida,[1,2,*] and Masanori Ozaki[1]

[1]*Division of Electrical, Electronic and Information Engineering, Graduate School of Engineering, Osaka University,*
2-1 Yamada-oka, Suita, Osaka 565-0871, Japan
[2]*PRESTO, Japan Science and Technology Agency (JST), 4-1-8 Honcho, Kawaguchi, Saitama 332-0012, Japan*

Recent studies on topological defects in conventional and active nematic liquid crystals have revealed their potential as sources of advanced functionality whereby the collective behavior of the constituent molecules or cells is controlled. On the other hand, the fact that they have high energies and are metastable makes their shape control a nontrivial issue. Here, we demonstrate stabilization of arbitrary-shaped closed disclination loops with 1/2 strength floating in the bulk by designing the twist angle distribution in a liquid crystal cell. Continuous variation of the twist angle from below to above $|\pi/2|$ allows us to unambiguously position reverse twist disclinations at will. We also analyze the elastic free energy and uncover the relationship between the twist angle pattern and shrink rate of the surface-stabilized disclination loop.

The orientation of the nematic liquid crystal (LC) phase exhibited by small rodlike molecules is described by the so-called director, a unit vector with head-tail symmetry orientated along the common average direction [1]. Topological defects appear in nematic LCs as points or lines where the continuous rotational symmetry of the director is broken. They have recently attracted strong interest because of their unique behavior distinct from LCs aligned in the bulk [1–3]. Defects mediate spin-orbit interaction of light, leading to spin-angular-momentum-dependent generation of optical vortices [4]. They also change the rheological properties of the LC [5,6], lead to novel photomechanical phenomena [7,8], and can act as templates to position colloidal materials [9–12]. More recently, it has been demonstrated that defects can localize guest molecules (i.e., not just colloidal particles with sizes much larger than the LC molecules) and promote self-association [13–16].

The reports on the various functions suggest that defects can become more than just imperfections in the alignment. However, to exploit their potential as sources of functionality, control of their shapes is necessary. Shape control of defects is challenging because defects have high energies and thus are in general metastable. There are two main approaches to stabilize defects in LCs; either to dope colloidal particles [17–21] or to impose spatially designed boundary conditions [12,22–25]. Colloidal inclusions generate topological defects following the Gauss-Bonnét and Poincaré-Hopf theorems of topology, and extremely complex defects such as those with linked or knotted structures have been generated. However, defects generated by particles are bound close to the particle surface and thus their shapes are defined almost exclusively by the shapes of the particles. Defect shape control through surface anchoring can provide larger freedom in the achievable shapes. Line defects running through the LC bulk have been generated by imprinting

_____
*Corresponding author: yoshida@eei.eng.osaka-u.ac.jp

singular points in the easy axis distribution on the substrates, and recently, a web of defect lines has been demonstrated by creating orthogonal linear gradients in the easy axis of two substrates [25]. However, the shape control of a closed single loop had not been demonstrated.

In this Rapid Communication, we describe a general protocol to generate loop defects with arbitrary shape floating in a slab of nematic LC. The method uses a unidirectionally orientated substrate in combination with a substrate with patterned easy axis distribution, so that a position-dependent twist is induced in the bulk director. The achirality of the nematic LC imposes the condition that the twist sense be such that the twist angle is minimized, and where the twist angle exceeds $|\pi/2|$, a twist reversal occurs, accompanied by the generation of a twist disclination [12,25]. By continuously varying the easy axis from below to above $|\pi/2|$, the exact position at which twist reversal should occur can be defined, leading to a stable closed loop.

Figure 1(a) schematically illustrates the easy axis design for generating a circular defect loop, where the tangent of the streamlines represents the local director orientation. The easy axis on the patterned substrate, $\varphi_p(r)$, is given by Eq. (1), where we have employed cylindrical coordinates in consideration of the symmetry of the loop. The origin is placed at the center of the pattern, and r is the position from the center of the pattern:

$$\varphi_p(r) = \begin{cases} 0, & r < r_0 - a \\ \frac{r+a-r_0}{2a}\pi, & r_0 - a \leqslant r \leqslant r_0 + a \\ 0, & r > r_0 + a. \end{cases} \quad (1)$$

The easy axis rotates linearly by π over a distance of $2a$, where r_0 is the position at which the twist angle is $\pi/2$. When a unidirectionally orientated substrate with orientation along 0 radians [Fig. 1(b)] is used to assemble a sandwich cell, the same expression also describes the twist angle distribution in the cell [Fig. 1(c)]. However, the achirality condition of the nematic LC causes the twist angle to be wrapped to between $-\pi/2$ and $\pi/2$; the defect should
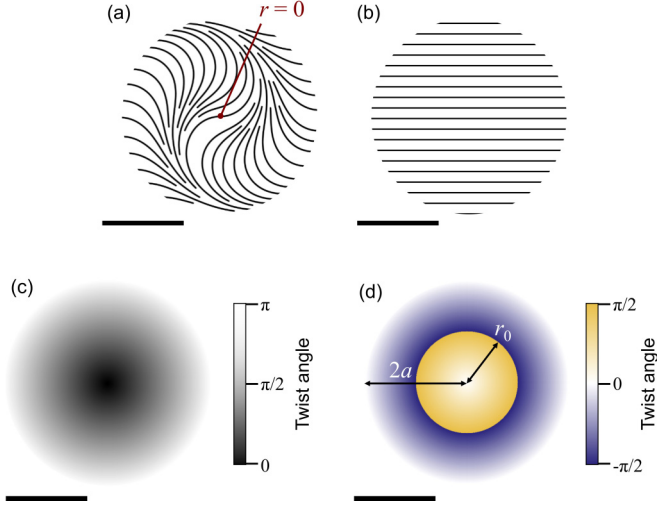
FIG. 1. Schematic illustrations of the orientational easy axis distributions on (a) patterned and (b) planar substrates to generate a loop defect. (c) Twist angle distribution of the LC director between the substrates. (d) Twist angle distribution considering twist reversal in the bulk. Scale bars in the figure indicate 100 μm when the design parameters are $r_0 = a = 66 \mu$m. Note that when $a < r_0$, a circular region with unidirectional orientation appears at the center.

appear at the phase discontinuity, which is at $r = r_0$ for this design [Fig. 1(d)].

A sandwich cell is experimentally fabricated to confirm the generation of loop defects. The uniform planar substrate is prepared by coating a planar-orientation agent (JSR, AL1254) and rubbing it unidirectionally. The patterned planar substrate is prepared by coating a photoalignment agent (DIC, LIA-03). The substrates were first assembled into a sandwich cell with a cell gap of approximately 6 μm, and then the easy axis distribution was imprinted on the patterned substrate using a maskless photoalignment setup [26]. A LC display projector was used as an electronic mask to control the spatial pattern of light, and the light was irradiated sequentially on the sample after controlling the polarization. The system has a resolution of 1024×768 pixels with an approximate pixel size on the sample of $1.3 \times 1.3 \mu$m^2. The easy axis pattern was imprinted

on the substrate at an interval of $1°$, with light dosage of 45 μJ per pixel.

For observation, a nematic LC (5CB, Merck) was filled into the cell in the isotropic phase and slowly cooled down to the nematic phase. As the LC entered the nematic phase, a disclination appeared close to the patterned region, and relaxed to form a loop. Figure 2 shows polarizing optical microscope (POM) images of the sample with design parameters $r_0 = a = 66$ μm. The transmittance of the cell between crossed polarizers is highest at approximately $r = r_0$ and is symmetric about this position, implying that the twist angle distribution is symmetric. The disclination loop is observed as a thin dark line floating in the bright background near r_0, and is observable also when the analyzer is removed because of light scattering [Fig. 2(b)]. Insertion of a retardation plate (530 nm, inserted at $45°$ to the crossed polarizers) confirms that the twist sense is, in fact, reversed at this disclination to reduce the twist angle. Judging from the interference colors in Fig. 2(c), the twist angle sense is right (left) -handed inside (outside) the loop, corresponding to the design of Fig. 1.

Disclination loops similar to the one in Fig. 2 can also appear randomly at the isotropic-nematic phase transition in a twisted nematic cell with twist angle of $|\pi/2|$. However, the high energy of the disclination exerts a tension on the loop and makes it metastable to shrink typically within seconds [1,27]. The disclination generated here also experiences a tension, but is stabilized by the anchoring conditions imposed on the substrates [12,25]. This means that in contrast to disclinations in uniform cells, the loop reappears and settles at the same position when the material is heated to above the clearing point and then cooled back down.

The existence of a tension can be observed by measuring the deviation of its length from the designed length. The expected length of the loop in Fig. 2 was 415 μm($= 2\pi r_0$), whereas the observed length was 342 μm. To investigate the relationship between the easy axis pattern and shrink rate of the loop defect, various patterns were created as functions of the pattern width (a) and twist reversal position (r_0), and compared with designed loop length.

Figure 3 shows the measured and designed lengths of disclinations for various design parameters. The experiments were carried out in three independent samples, and the average lengths are plotted. In Fig. 3(a), the change in pattern width
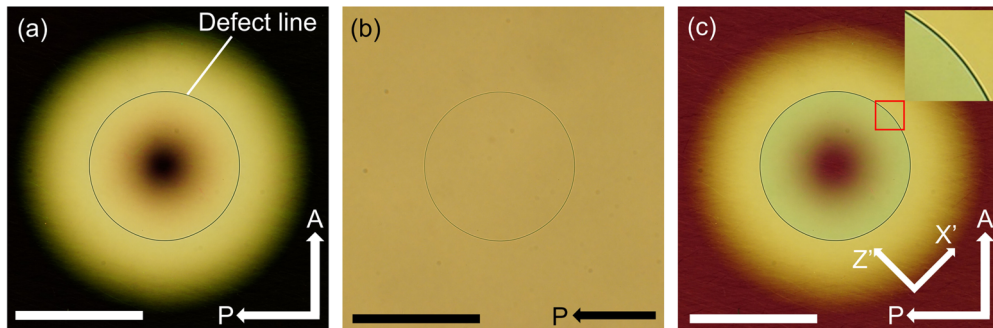

FIG. 2. POM images of loop defects observed (a) between crossed polarizers, (b) without analyzer, and (c) with a 530 nm retardation plate inserted in the optical path (X' and Z' indicate the fast and slow axes of the plate, respectively). The region inside the disclination has a green tint, while the region outside has yellow tint. Arrow labels P and A indicate the directions of polarizer and analyzer, respectively. Scale bars: 100 μm.
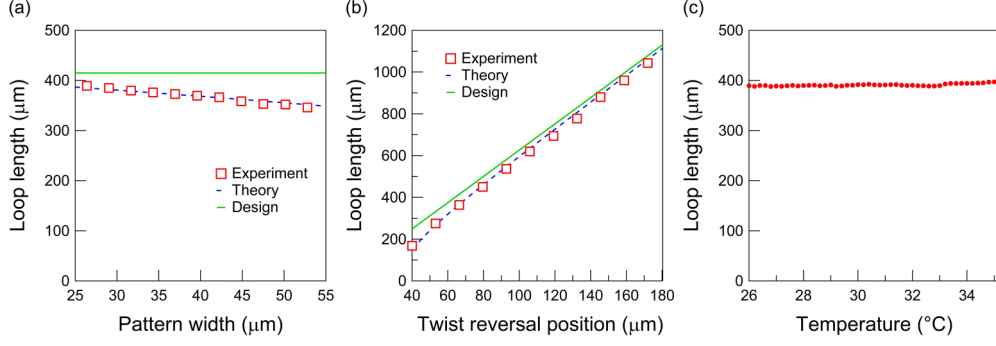
FIG. 3. Experimental, theoretical, and designed loop lengths as a function of (a) pattern width a and (b) twist reversal position r_0. Measurements were made for three independent samples. (c) Temperature dependence of the loop length in the sample with design parameters $r_0 = 66$ μm and $a = 26.4$ μm.

does not affect the designed loop length; however, the loop length approaches the designed length as the pattern width becomes narrower. From Fig. 3(b), the loop length approaches the designed length as the twist reversal position becomes larger.

To gain a physical understanding of the phenomenon, we theoretically analyze the free energy of the system. As mentioned earlier, the disclination experiences a line tension because of the high energy, and there is always a tendency to reduce its length. As the defect shrinks, however, the director deviates from the most stable state imposed by the surface anchoring conditions and increases in elastic energy. The equilibrium position of the loop should be where these two competing forces are balanced.

We first calculate the gain in elastic free energy due to loop shrinkage. Considering the symmetry of the loop and twist angle distribution, we model the system using cylindrical coordinates. By definition of the twist disclination, the twist sense reverses only at the disclination; however, from Fig. 2(c), the director twist appears to be continuous up to the disclination line, even when the loop has shrunk from its designed position. This implies that when loop shrinkage occurs, the director no longer reverses its twist sense at twist angles of $\pm\pi/2$, but at angles $(\pi/2 - \delta)$ and $-(\pi/2 + \delta)$, where the deviation angle, δ, is defined by the boundary conditions at the position of twist reversal. From Fig. 2(c) and the fact that the two substrates have sufficiently small pretilt angles (1.4° and 0.1° for the rubbing and photoalignment cells, respectively [28]), we further assume that there is no tilt induced (i.e., the director always lies parallel to the substrates), and express the director distribution, $\mathbf{n}$, as $\mathbf{n} = [\cos\varphi(r,z), \sin\varphi(r,z), 0]$, where $\varphi(r,z)$ is given by the following expression:

$$\varphi(r,z) = \begin{cases} 0, & r < r_0 - a \\ \frac{\pi}{2a}(r - a + r_0)\frac{z}{d}, & r_0 - a \leqslant r < (1-\alpha)r_0 \\ \frac{\pi}{2a}(r - a - r_0)\frac{z}{d}, & (1-\alpha)r_0 < r \leqslant r_0 + a \\ 0, & r > r_0 + a. \end{cases} \quad (2)$$

Here, d is the cell gap where we have assumed the two substrate surfaces to exist at $z = 0$ (planar substrate) and d (patterned substrate), and α ($0 \leqslant \alpha \leqslant 1$) is the shrink rate of the loop. Note that $\varphi(r,d) = \varphi_{\mathrm{p}}(r)$.

The elastic free energy of LCs is related to three different deformation modes of the director with different elastic constants (K_{11} for splay, K_{22} for twist, and K_{33} for bend deformations, respectively). For an analytical understanding of the system, we employ the one-constant approximation where the three elastic constants are assumed to be equal ($K = K_{11} = K_{22} = K_{33}$), and obtain an analytical expression for the free energy:

$$\begin{aligned} F_{\mathrm{EL}} &= \int \frac{1}{2}K\left\{ \left(\frac{\partial\varphi}{\partial r}\right)^2 + \left(\frac{\partial\varphi}{\partial z}\right)^2 + \frac{1}{r^2} \right\}dV \\ &= \frac{K\pi^2 r_0 d}{6a} + \frac{K\pi^3}{2da^2}\left\{ \frac{2}{3}(1-\alpha)^3 r_0^3 a - (1-\alpha)^2 r_0^3 a \right. \\ &\quad \left. + \frac{1}{3}r_0^3 w(r_0^2 + a^2) \right\} + K\pi d \ln\frac{r_0 + a}{r_0 - a}. \end{aligned} \quad (3)$$

The change in free energy as the loop shrinks from the designed position is given by Eq. (4), which is always positive for $0 \leqslant \alpha \leqslant 1$.

$$\Delta F_{\mathrm{EL}} = F_{\mathrm{EL}} - F_{\mathrm{EL}}|_{\alpha=0} = \frac{K\pi^3 r_0^3}{2da}\alpha^2\left(1 - \frac{2}{3}\alpha\right). \quad (4)$$

The free energy of the disclination core is expressed as a combination of the core and interfacial energies, following the treatment by Wang *et al.* [29]:

$$F_{\mathrm{D}} = 2\pi r_0(1-\alpha)\left\{ \left(\pi r_c^2 \varepsilon_c\right)_{\mathrm{core}} + \left[2\pi r_c \sigma_c\left(1 + \frac{w}{2}\right)\right]_{\mathrm{surface}} \right\}. \quad (5)$$

Here, r_c is the radius of defect core, ε_c is the free energy density of defect core, σ_c is the isotropic-nematic interfacial tension, and w is the surface anchoring energy coefficient [2,6,30]. Note that we have omitted the elastic energy of director deformation in the vicinity of the defect because we have defined the orientation through the boundary conditions. As the loop shrinks, the energy of the disclination decreases as follows:

$$\Delta F_{\mathrm{EL}} = F_{\mathrm{EL}} - F_{\mathrm{EL}}|_{\alpha=0} = \frac{K\pi^3 r_0^3}{2da}\alpha^2\left(1 - \frac{2}{3}\alpha\right). \quad (6)$$
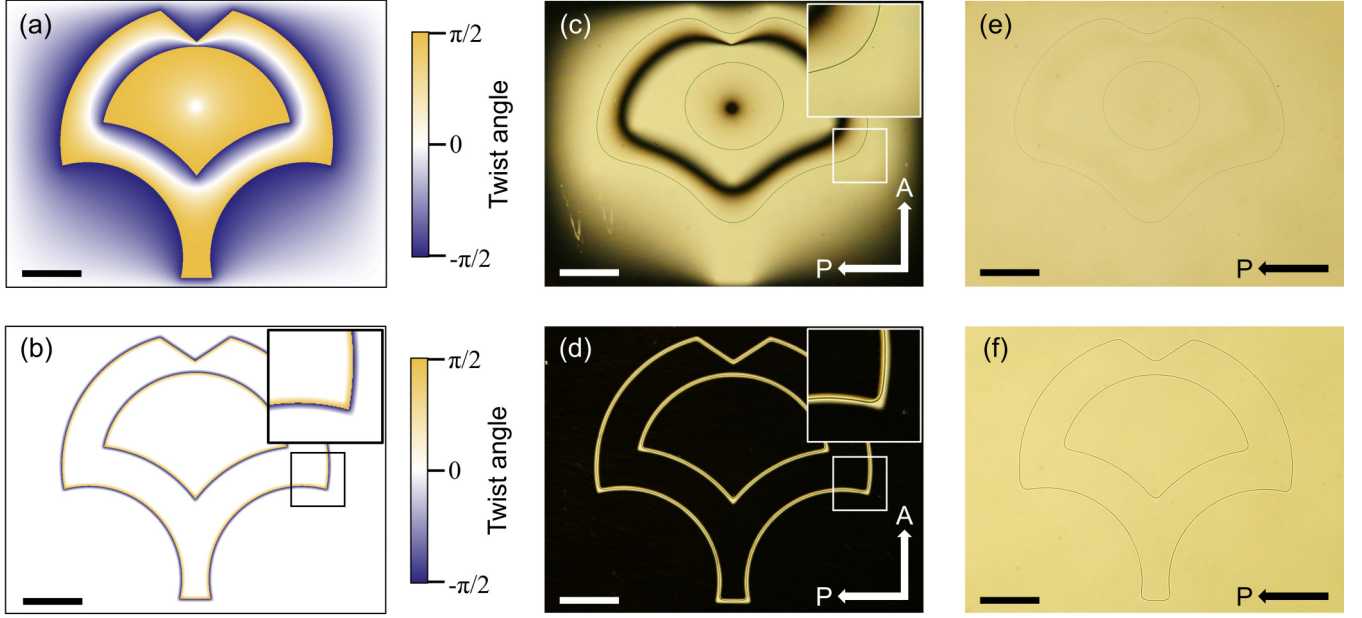
FIG. 4. Twist angle distributions to generate disclination loops resembling the Osaka University logo obtained by (a) solving Laplace's equation as a boundary problem in each region boundary, and (b) creating an outline with a width of 13 μm and varying the angle from 0 to π. (c),(e) POM images of the disclination lines generated by pattern (a), and (d),(f) POM images of the disclination lines generated by pattern (b). Scale bars: 200 μm.

The equilibrium shrink rate of the loop is found by placing $\Delta F_{\mathrm{EL}} = \Delta F_{\mathrm{D}}$:

$$\alpha = \frac{3}{4} - \sqrt{\frac{9}{16} - \frac{6da}{K\pi r_0^2}\left\{r_c^2\varepsilon_c + 2r_c\sigma_c\left(1 + \frac{w}{2}\right)\right\}}. \quad (7)$$

Equation (7) explicitly describes the relationship between the loop radius and design parameters. In Fig. 3, the theoretical loop lengths are plotted as blue dashed curves, using the following parameters: $K = 6.26$ pN, $r_c = 14$ nm, $\varepsilon_c = 5 \times 10^4$ J/m^3, $\sigma_c = 10^{-5}$ J/m^2, $w = 10^{-2}$, and $d = 5.5$ μm and $r_0 = 66$ μm for (a), and $d = 5.81$ μm and $a = 39.6$ μm for (b). Although many of the parameters concerning the defect core are difficult to evaluate experimentally, good agreement is observed between experiment and theory using values close to those reported in the literature [31]. Importantly, the same material parameters reproduce the experimental results for the two independent experiments in Fig. 3.

Here, analytical treatment of the free energies has been made possible by ignoring the elastic anisotropy and using a symmetric pattern. In standard nematics, typically $K_{11} \approx K_{33} \approx 2K_{22}$; however, the agreement of our simplified theory with experiment implies that the effect of elastic anisotropy is not significant to cause a drastic deviation in the theoretical loop length in the lengths of several hundred micrometers studied here. This is also supported from the small temperature dependence of the loop length, as shown in Fig. 3(c).

As the pattern deviates from that for the circular loop, it will become necessary to perform numerical simulations to predict the degree of shrinkage. However, the proposed principle can be applied as a general guide to stabilize disclination loops of arbitrary shapes; a sufficiently narrow, linearly modulated

easy axis pattern around the desired position of the disclination should surface stabilize the loop. As an example, Fig. 4 shows double disclination loops forming the Osaka University logo. To demonstrate the difference in disclination shrinkage depending on pattern, two kinds of easy axis patterns are prepared: one with a smooth distribution, obtained by solving Laplace's equation as a boundary problem in each region bounded by the disclination loop [assuming values of $\pm\pi/2$ at each side of the boundaries and at the center of the logo, Fig. 4(a)]; and another distribution creating an outline with a width of 13 μm around each line composing the logo and varying the angle from 0 to π [Fig. 4(b)]. Figures 4(c)–4(f) show POM images of double disclination loops. The disclination lines generated by the pattern of Fig. 4(a) shows large shrinkage such that the disclinations almost become circular [Figs. 4(c) and 4(e)]. On the other hand, disclinations generated from the pattern of Fig. 4(b) maintain the designed shapes [Figs. 4(d) and 4(f)], with shrinkage only seen at the corners. The proposed principle thus enables disclinations to be manipulated to resemble meaningful symbols.

In conclusion, we have experimentally demonstrated stabilization of disclination loops floating in a nematic LC by designing the twist angle distribution between two substrates. The line tension of the disclination can be counterbalanced by creating a continuous variation in the left- and right-handed twist angles in the vicinity of the disclination. A narrower distribution effectively increases the elasticity of the bulk LC, suppressing shrinkage. So far, we have only been able to stabilize simple loops with no knots or links with this method; however, the addition of chirality in the nematic may lead to stabilization of defects with more complex topologies [31]. While a growing number of studies are reporting novel functions in

LC defects, the study on defects is inherently difficult due to their metastable characteristics. The development of defect stabilization methods such as the one proposed here will enable in-depth studies of their properties such as dynamics [32] and interactions with matter, potentially leading to applications in optics, materials, and biology.

[1] S. Chandrasekhar, *Liquid Crystals*, 2nd ed. (Cambridge University Press, Cambridge, UK, 1992).

[2] O. D. Lavrentovich, *Handbook of Liquid Crystals*, 2nd ed. (Wiley-VCH Verlag Gmbh & Co. KGaA, Weinheim, 2014), Chap. 6.

[3] N. Schopohl and T. J. Sluckin, Phys. Rev. Lett. **59**, 2582 (1987).

[4] L. Marrucci, C. Manzo, and D. Paparo, Phys. Rev. Lett. **96**, 163905 (2006).

[5] M. Zapotocky, L. Ramos, P. Poulin, T. C. Lubensky, and D. A. Weitz, Science **283**, 209 (1999).

[6] Y.-K. Kim, S. V. Shiyanovskii, and O. D. Lavrentovich, J. Phys.: Condens. Matter **25**, 404202 (2013).

[7] T. H. Ware, M. E. McConney, J. J. Wie, V. P. Tondiglia, and T. J. White, Science **347**, 982 (2015).

[8] T. J. White and D. J. Broer, Nat. Mater. **14**, 1087 (2015).

[9] I. Muševič, M. Škarabot, U. Tkalec, M. Ravnik, and S. Žumer, Science **313**, 954 (2006).

[10] B. Senyuk, J. S. Evans, P. J. Ackerman, T. Lee, P. Manna, L. Vigderman, E. R. Zubarev, J. van de Lagemaat, and I. I. Smalyukh, Nano Lett. **12**, 955 (2012).

[11] J. B. Fleury, D. Pires, and Y. Galerne, Phys. Rev. Lett. **103**, 267801 (2009).

[12] H. Yoshida, K. Asakura, J. Fukuda, and M. Ozaki, Nat. Commun. **6**, 7180 (2015).

[13] X. Wang, D. S. Miller, E. Bukusoglu, J. J. de Pablo, and N. L. Abbott, Nat. Mater. **15**. 106 (2016).

[14] T. Ohzono, K. Katoh, and J. Fukuda, Sci. Rep. **6**, 36477 (2016).

[15] T. B. Saw, A. Doostmohammadi, V. Nier, L. Kocgozlu, S. Thampi, Y. Toyama, P. Marcq, C. T. Lim, J. M. Yeomans, and B. Ladoux, Nature (London) **544**, 212 (2017).

[16] K. Kawaguchi, R. Kageyama, and M. Sano, Nature (London) **545**, 327 (2017).

[17] U. Tkalec, M. Ravnik, S. Copar, S. Zumer, and I. Musevic, Science **333**, 62 (2011).

[18] B. Senyuk, Q. Liu, S. He, R. D. Kamien, R. B. Kusner, T. C. Lubensky, and I. I. Smalyukh, Nature (London) **493**, 200 (2013).

[19] A. Martinez, M. Ravnik, B. Lucero, R. Visvanathan, S. Zumer, and I. I. Smalyukh, Nat. Mater. **13**, 258 (2014).

[20] S. Copar and S. Žumer, Proc. Natl. Acad. Sci. U.S.A. **112**, 1675 (2015).

[21] Y. Yuan, A. Martinez, B. Senyuk, M. Tasinkevych, and I. I. Smalyukh, Nat. Mater. **17**, 71 (2018).

[22] T. Ohzono and J. Fukuda, Nat. Commun. **3**, 701 (2012).

[23] B. S. Murray, R. A. Pelcovits, and C. Rosenblatt, Phys. Rev. E **90**, 052501 (2014).

[24] D. Kasyanyuk, P. Pagliusi, A. Mazzulla, V. Reshetnyak, Y. Reznikov, C. Provenzano, M. Giocondo, M. Vasnetsov, O. Yaroshchuk, and G. Cipparrone, Sci. Rep. **6**, 20742 (2016).

[25] M. Wang, Y. Li, and H. Yokoyama, Nat. Commun. **8**, 388 (2017).

[26] J. Kobashi, H. Yoshida, and M. Ozaki, Nat. Photonics **10**, 389 (2016).

[27] I. Chuang, N. Turok, and B. Yurke, Phys. Rev. Lett. **66**, 2472 (1991).

[28] M. Takahashi, T. Ohkawa, H. Yoshida, J. Fukuda, H. Kikuchi, and M. Ozaki, J. Phys. D: Appl. Phys. (2018), doi: 10.1088/1361-6463/aaaa4b.

[29] X. Wang, Y. K. Kim, E. Bukusoglu, B. Zhang, D. S. Miller, and N. L. Abbott, Phys. Rev. Lett. **116**, 147801 (2016).

[30] E. M. Terentjev, Phys. Rev. E **51**, 1330 (1995).

[31] T. Machon and G. P. Alexander, Phys. Rev. Lett. **113**, 027801 (2014).

[32] N. Osterman, J. Kotar, E. M. Terentjev, and P. Cicuta, Phys. Rev. E **81**, 061701 (2010).